JOURNAL OF SYNCHROTRON RADIATION
ISSN 1600-5775

Upgrade of BL-5C as a highly automated macromolecular crystallography beamline at Pohang Light Source II

Jae-Hee Jeong,‡ Cheolsoo Eo,‡ Hyo-Yun Kim, Jin-Hong Kim, Chae-Soon Lee, Hyeong-Joo Choi and Yeon-Gil Kim*

Beamline Science, Pohang Accelerator Laboratory, 80 Jigokro-127-beongil, Pohang, Kyungbuk 37673, Republic of Korea. *Correspondence e-mail: ygkim76@postech.ac.kr

Received 13 November 2020
Accepted 17 January 2021

Edited by Y. Amemiya, University of Tokyo, Japan

‡ These authors contributed equally to this work.

Keywords: macromolecular crystallography; beamline automation; high-throughput.

BL-5C is an in-vacuum undulator beamline dedicated to macromolecular crystallography (MX) at the 3 GeV Pohang Light Source II in Korea. The beamline delivers X-ray beams with a focal spot size of 200 µm × 40 µm (FWHM, H × V) over the energy range 6.5–16.5 keV. The measured flux is 7×10^{11} photons s^{-1} at 12.659 keV through an aperture size of 50 µm. The experimental station is newly equipped with the photon-counting detector EIGER 9M, the multi-axis micro-diffractometer MD2, and a robotic sample changer with a high-capacity dewar. These instruments enable the operation of this beamline as an automated MX beamline specialized in X-ray fragment screening. This beamline can collect more than 400 data sets a day without human intervention, and a difference map can be automatically calculated by using the data processing pipeline for ligand or fragment identification.

1. Introduction

Pohang Light Source II (PLS-II) is a third-generation synchrotron source located at the campus of Pohang University of Science and Technology (POSTECH) in Korea. PLS-II operates at an electron energy of 3.0 GeV in top-up mode with stored currents up to 400 mA (Hwang *et al.*, 2014). The 36 beamlines at PLS-II are operating to serve the user community with a wide range of applications in physics, chemistry, and life sciences. Among them, three undulator beamlines (BL-5C, BL-7A, and BL-11C) are assigned for macromolecular crystallography (MX) to support the structural biology community in academia and industry. To date, the three MX beamlines have contributed to determine more than 1906 protein structures [http://biosync.sbkb.org/ (accessed on 4 November 2020)]. The two beamlines BL-5C and BL-7A have a simple experimental configuration equipped with a Crystal Logic goniostat (Crystal Logic, LA, USA) combined with an ADSC CCD detector (ADSC, USA), and provide only manual mounting mode. Although they have largely contributed to crystal structure determination for domestic users, the development has been delayed. The BL-11C beamline, equipped with the robotic sample mounting system CATS (IRELEC, France) and the photon-counting detector Pilatu 6M (Dectris, Switzerland), was introduced to the user community in June 2017. The main purpose of BL-11C is to determine crystal structures from weakly diffracting microcrystals less than 10 µm in size that cannot be determined at the other two beamlines.

Recently, MX beamlines at many of synchrotron facilities worldwide, such as SPring-8, ESRF, Diamond Light Source,

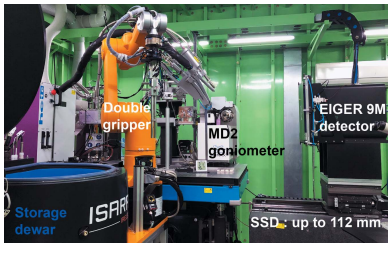

and Advance Photon Source, were transformed to be operated as fully automated systems (Bowler *et al.*, 2015; Cianci *et al.*, 2017; Wasserman *et al.*, 2012; Sanchez-Weatherby *et al.*, 2019; Hirata *et al.*, 2019). The speed of data collection of these MX beamlines is $\geq$20 crystals per hour owing to the introduction of pixel-array detectors and the use of a robot. Based on these developments, some beamlines are routinely used to screen a thousand fragments by applying high-throughput data collection (Bradley *et al.*, 2018; Lima *et al.*, 2020). Domestic user communities also demanded fully automated and high-throughput MX beamlines specialized in X-ray fragment screening that uses large and single well diffracting crystals. The targeted crystal size of BL-5C is larger than 50 µm in diameter, suitable for the ligand and fragment screening. For these reasons, BL-5C has been intensively developed over the last two years into a highly automated MX beamline that conducts sample mounting, crystal centering, data collection from a single crystal, and data analysis under unattended mode. The experimental station of BL-5C was completely rebuilt by installing an EIGER 9M detector (Dectris, Switzerland), an MD2 micro-diffractometer (ARINAX, France), and a robotic sample changer ISARA (IRELEC, France). The beamline control system and user software environment of BL-5C were also renovated to maximize the throughput of data collection and to accelerate hit identification based on full automation of crystallographic diffraction experiments. BL-5C is now capable of collecting data sets from a large number of crystals, and allows remote access to the beamline.

2. Beamline overview

2.1. Photon source and front-end

The photon source of BL-5C is a hybrid-type in-vacuum undulator (IVU) of length 1.4 m comprising 67 periods, each with length 20 mm (SFA, Korea). The undulator can provide up to 2.95 kW of X-ray power under PLS-II operating parameters (electron energy of 3.0 GeV and beam currents of 400 mA) (Yu *et al.*, 2014). It has a working gap range of 5 to 16 mm, and the available X-ray energy range is 5–20 keV utilizing the third to ninth odd harmonics. At the energy of 12.398 keV, the seventh harmonic is used at the gap range of 6.0 mm. The white beam from the undulator source passes the front-end (FE) section where a fixed mask (aperture size: 5 mm × 3 mm, H × V), a photon beam position monitor (PBPM), and a movable mask (aperture size: 0.8 mm × 0.4 mm, H × V) are placed in sequence. The fixed and movable masks can define a photon-beam acceptance angle and reduce the heat load of the downstream optical components. The PBPM constantly monitors the white beam position, which is used by a feedback system to control the photon-beam trajectory of the source (Ko *et al.*, 2016). The white-beam feedback system significantly contributes to the long-term beam stability of the beamline during a user service period. The FE section ends with a 200 µm-thick chemical-vapor-deposition diamond window that separates the storage ring vacuum from the other parts of the beamline. The window also acts as a high-pass filter removing photons with energy below ~5 keV, thus reducing the heat load on the downstream optical components. The beamline parameters are summarized in Table 1.

Table 1
Beamline details.

	After upgrade	Before upgrade
Year of operation	2020–	2005–2019
Source	–	IVU 20 1.4 m
Working energy range	–	6.5–16.5 keV
Beam size @ sample (FWHM, H × V)	–	200 µm × 40 µm
Flux @ 12.6 keV (photons s^{-1}) at default beam size†	–	7×10^{11} (50 µm)
Energy resolution	–	$\sim 1 \times 10^{-4}$
Monochromator	–	DCM Si (111), Kozhu
Detector distance (m)	–	0.11–0.6
Detector	EIGER 9M	ADSC Q315r
Sample changer	ISARA	Not available
Diffractometer	MD2	Crystal Logic
Goniometer	Multi-axis (ω, κ, φ)	Single-axis (ω)
Averaged exposure time per 1°	~0.2 s	~1 s
Data processing	*XDS* (automatic)	*HKL2000* (manual)

† Measurement performed using a silicon photodiode at a ring current of 250 mA.

2.2. Beamline optics

The main optical components of BL-5C are the vertically deflecting double-crystal silicon (111) monochromator (DCM) and the ellipsoidal focusing mirror system (Fig. 1). The polychromatic beam is monochromated ($\Delta E/E \simeq 10^{-4}$) by the DCM (Kozhu, Japan) located 18 m away from the light source.

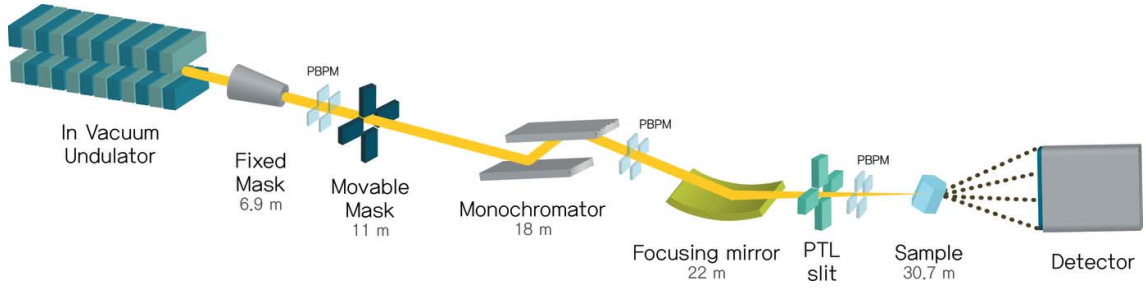

Figure 1
Schematic layout of the MX beamline BL-5C. Major components are shown with their distance relative to the undulator source.

The variable gap between two crystals maintains a fixed-exit beam offset of 25 mm when changing the wavelength. The two crystals are indirectly cooled by liquid nitrogen through a closed-loop liquid-nitrogen cooling system (Bruker, German) to diminish the heat load on the first crystal. Temperature sensors placed at various points in the DCM system monitor the thermal stability of the monochromator and communicate with the beamline interlock system to protect this important optical component from thermal damage. The monochromatic beam exiting the DCM is focused by a figured ellipsoidal mirror (JTEC, Japan) with an optical area of 580 mm (length) × 8 mm (width). The optical surface is coated with rhodium, and its surface roughness is within 3 Å (r.m.s). The tangential and sagittal slope errors are less than 0.5 µrad (r.m.s) and 2.0 µrad (r.m.s), respectively. The highly polished mirror with low slope error values will contribute to achieve a well focused beam by minimizing focal beam distortion. The mirror is located at 22.0 m from the source with a focusing ratio of 2.5:1, and the beam is focused into a spot size of dimensions 200 µm × 40 µm (FWHM, H × V) at a sample position of 30.7 m [Fig. 2(*a*)]. Through the default aperture size of 50 µm, the flux measured by a photodiode is 7×10^{11} photons s^{-1} at 12.6 keV under a storage ring current of 250 mA (Owen *et al.*, 2009). The available energy range of this beamline is between 6.5 keV and 16.5 keV for user experiments. The achieved beam properties are suitable for high-throughput crystallography.

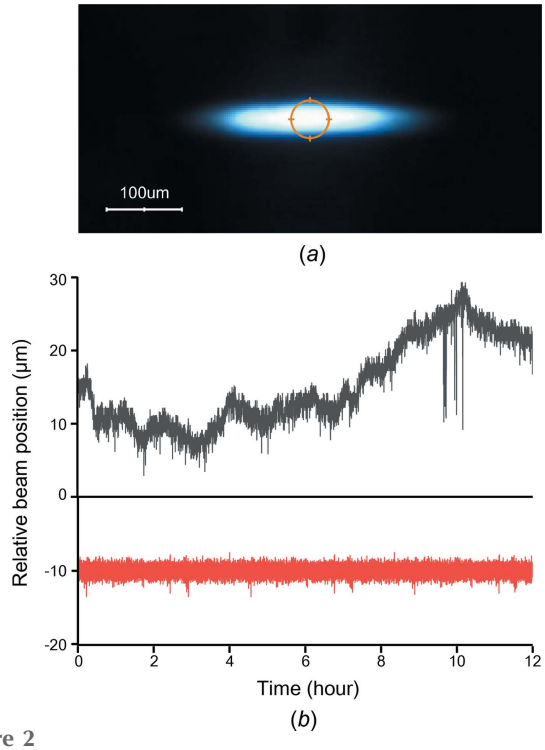

Figure 2
(*a*) Image of the fully focused beam at the sample position, determined with the built-in scintillator of MD2. (*b*) Beam stabilization of BL-5C with (red) or without (black) vertical-beam position feedback. The beam position with feedback was maintained for 12 h within ±3 µm displacement.

The X-ray beam stability is critical to obtain high-quality diffraction data in X-ray crystallography. Although PLS-II is operated under top-up mode, temperature changes of the experimental hall and refilling of the liquid-nitrogen container of the DCM cryocooler were reported to cause beam drift in the vertical direction at the sample position (Park *et al.*, 2018). To minimize this notorious effect, we implemented a vertical-beam position feedback system utilizing a piezo-electric device that tunes the second crystal of the DCM. The beam position of BL-5C is constantly monitored by the position-sensitive ionization chamber (PSIC) installed 1 m upstream of the sample position (Sato, 2001). The beam-position signal, with a data sampling rate of 120 Hz, is used for calculation of the feedback voltage to drive a piezo-electric actuator at the operational frequency of 2 Hz. When the feedback system is applied, the beam position at the sample remains unchanged within ±3 µm a day [Fig. 2(*b*)].

2.3. Experimental environment

The monochromatic beam exiting a beryllium window was monitored in terms of intensity and positions by the PSIC as described above. Then, the X-ray beam passes the beam attenuator (XIA, USA) composed of eight aluminium foils (0.01, 0.02, 0.04, 0.08, 0.16, 0.32, 0.64, and 1.5 mm in thickness, respectively) mounted on an individual pneumatic actuator. The X-ray beam attenuation can be regulated by the combination of various values of thickness of Al across the available energy range. The exposure of the X-ray beam to the sample is controlled by a fast electromagnetic shutter system (Bruker-AS) that uses an iron blade with an absorption length of 12 mm (2 mm vertical opening and 3 ms opening time).

The main equipment of the sample environment includes an MD2 micro-diffractometer (ARINAX, France), an EIGER X 9M detector (Dectris, Switzerland), a robotic sample changer ISARA (IRELEC, France), a CryoJet (Oxford Instruments, UK), and an HC1c (ARINAX, France) [Fig. 3(*a*)]. The MD2 micro-diffractometer plays an essential role in X-ray crystallographic experiments. The built-in accessories of the MD2, including an aperture set, a G-shaped capillary beamstop, and a YAG screen, are used for further conditioning of the incoming beam. The aperture set has five holes with sizes of 20, 30, 50, 75, and 100 µm for easy matching of the beam to the crystal size. The G-shaped capillary removes unwanted parasitic scattering by using a platinum plate presenting a pinhole of 150 µm at its center. The YAG screen can visualize the focused beam and can be used for probing the beam position and the alignment of the apertures and the capillary into the beam path.

The ready-to-use multi-axis (ω, κ, and φ) goniometer MK3 in the MD2 facilitates the data collection from large-unit-cell crystals [Fig. 3(*b*)] (Brockhauser *et al.*, 2013), though it has an increased sphere-of-confusion (SOC) of approximately 3 µm in comparison with that of a single-axis (ω) goniometer (SOC of 1 µm). The mounted crystal on the goniometer is visualized by an on-axis zoom microscope (0.23 µm $pixel^{-1}$ at maximum zoom) for crystal centering. The video frames generated by a

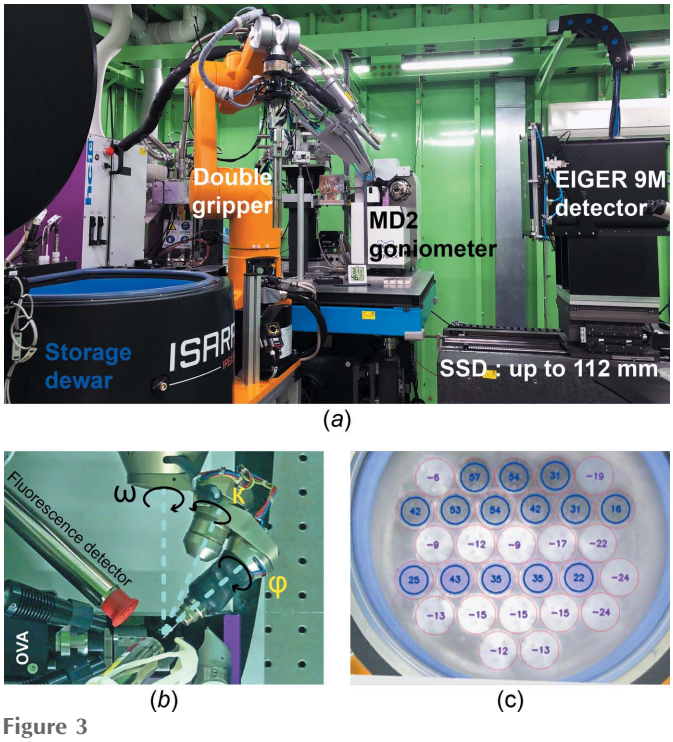

Figure 3
Experimental stations of BL-5C. (*a*) Photograph of the experimental hutch overview. (*b*) Close-up view of the sample environment at the centering mode equipped with a multi-axis goniometer. (*c*) Screenshot of the automatic puck tracking system that analyzes the dewar image to detect the puck (un)loading at the positions. The positive numbers indicate the relatively increased pixel intensity within the blue circles, and the presence of pucks.

prosilica GC655C GigE camera of the microscope are multicasted via the Vimba Viewer (Allied Visoin, German). The retractable Si-PIN photodiode detector XR-100CR (Amptek, USA) mounted on the MD2 is used for conducting the X-ray absorption near-edge structure (XANES) scan for multi-wavelength anomalous diffraction experiments or X-ray fluorescence measurement for identification of heavy atoms. The result from the XANES scan is automatically processed with *CHOOCH* (Evans & Pettifer, 2001).

The recently installed EIGER 9M detector offers a sensitive area (233.2 mm × 245.2 mm), a fast framing rate (238 Hz), a large image bit-depth (32), a point-spread function of 1 pixel, and the possibility of applying an energy threshold to the data collection. The detector can be activated via a hardware trigger that is generated from the MD2 controller based on the angular position of the rotation axis. These features can enable the implementation of a fine-slicing data collection method, a helical data collection method, and raster scan capabilities in BL-5C (Casanas *et al.*, 2016). The detector stage provides three directions of linear-translational movement; one of them is used for changing the sample–detector distance from 112 to 600 mm. The sensitive area of the detector is protected from mechanical damage by using a detector cover that is interlocked to the hutch door.

The robotic sample changer ISARA plays an important role in the efficient data collection and/or crystal screens via either remote access or on-site experiments. The ISARA features a six-axis robot arm (STÄUBLI, Switzerland) and a large sample dewar. The double gripper system, which is designed for grabbing SPINE sample pins through a magnetic force, allows a fast sample-exchange time below 15 s. The storage dewar of the robot can store up to 464 samples in 29 UniPuck containers. The large number of pucks can cause human mistakes during puck (un)loading, so we developed a puck tracking system. In the system, the dewar image taken from the surveillance camera in the hutch is analyzed to determine the presence or absence of pucks by calculating the averaged pixel intensity at the given 29 puck positions [Fig. 3(*c*)]. In addition, users or staff have to provide UniPuck's label to the system by scanning the engraved Data Matrix or QR code using a barcode reader just after (un)loading the puck in the dewar. At the same time, the barcode reading activates the dewar image processing. Then the puck tracking system can detect where the newly loaded puck is located in the dewar or which pucks are removed from the dewar. The result is automatically updated to the database system managing the puck lists for robot operation.

The Cryojet XL system keeps the crystals at 100 K in standard operation and the nozzle is equipped with an annealing system (Giraud *et al.*, 2009). In addition, a humidity controller device HC1c can be used to find the best dehydration condition by adjusting the humidity around crystals. Thereby, the diffraction quality and/or resolution of dehydrated crystals can be improved. The crystal can be flash-cooled directly with the CryoJet nozzle by using an in-house developed nozzle exchanger for full data collection.

2.4. Software

An experimental physics and industrial control system (EPICS) was used to control all motors and devices at the BL-5C beamline through input–output controllers (IOCs) (Dalesio *et al.*, 1994). This allows for distributed control of beamline components via a local network. Data acquisition software for users requires an integrated control of the beamline and an intuitive graphical user interface (GUI) for MX experiments. *MxDC* and *MxLIVE* developed at the Canadian Light Source (CLS) were introduced into BL-5C as end-user software (Fodje *et al.*, 2012), and adapted to the environment of BL-5C (Fig. 4). *MxLIVE* is a web-based experimental management system for users through which the sample lists for the robotic sample changer can be submitted. *MxDC* provides access to the sample centering, experimental setup, data collection, fluorescence scan, and sample changer operation. *MxDC* features an automatic data collection procedure through which sample mount, crystal centering, and data collection can be sequentially performed without human intervention. The automated procedure is particularly useful for the high-throughput fragment and ligand screening in which well characterized crystals are used. The crystal-centering task, which is the most important step for automation, consists of two steps: a loop-centering step based on optical image analysis, and an X-ray centering step based on diffraction analysis after raster scans at two perpendicular

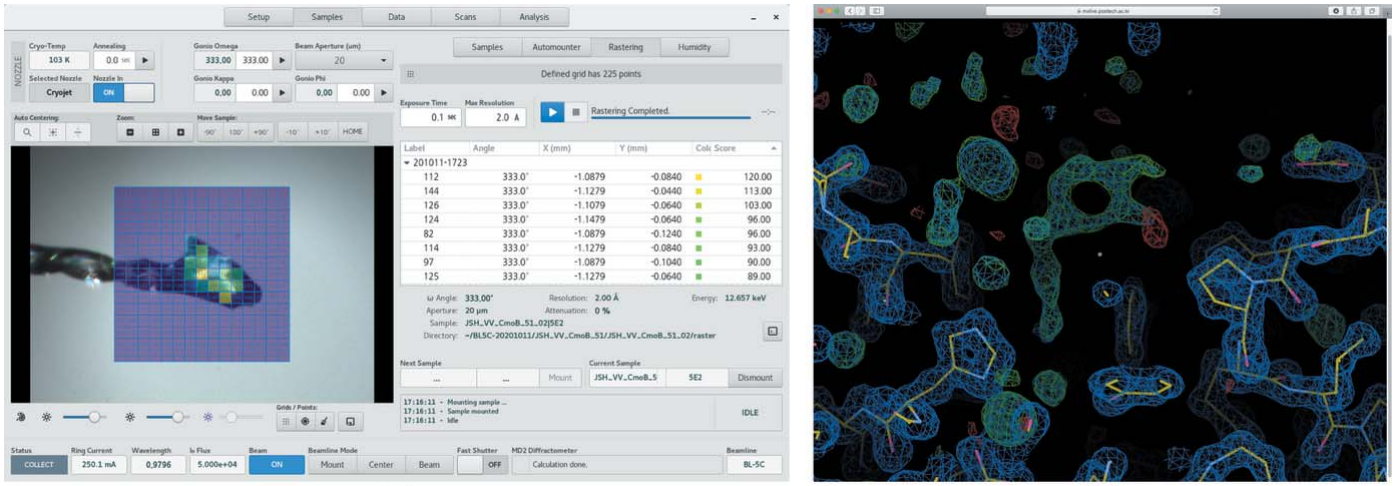

(*a*) (*b*)

Figure 4
User software environments. (*a*) Screenshot of the *MxDC* GUI showing the raster scan result in the sample tap. The raster scan for the crystal was performed with an aperture size of 20 µm at 10 Hz (oscillation angle, 0.1°; exposure time, 0.1 s; transmission 20%). The scores of each frame calculated by *dials.find_spots* are shown in a heat map where yellow represents the strongest diffraction. (*b*) Screenshot of *UglyMol* in the *MxLIVE* webpage showing the $F_o - F_c$ difference map representing the bound ligand in the target protein. The $F_o - F_c$ and $2F_o - F_c$ density maps contoured at 1.5σ at a resolution of 2.1 Å are shown in green and blue, respectively.

angles. By default, the first raster scan at the loop face angle is performed over an area of 300 µm × 300 µm corresponding to a 15 × 15 grid (horizontal × vertical). The serial images from the raster scan are interpreted by *dials.find_spots* (Winter *et al.*, 2018), and the best diffraction region is moved to the center [Fig. 4(*a*)]. The second raster scan after rotation of 90° is performed with a 3 × 15 grid in order to locate the crystal at the beam center over the full rotation range. The automatic crystal centering system based on the fast-raster scan method has been widely implemented at MX beamlines utilizing a fast-readout detector (Hirata *et al.*, 2019; Wojdyla *et al.*, 2016; Bowler *et al.*, 2016). In our system, the automatic crystal centering is typically conducted within 100 s. The next step is the automatic full data collection where the experimental parameters have to be specified in advance by users who know the properties of the crystals. In most of our X-ray fragment screening experiments, diffraction data were collected with a total rotation range of 240° within 48 s by using an aperture size of 50 µm or 75 µm at 100% transmission. Consequently, full data-set collection including sample exchange and crystal centering under an automated mode takes approximately 200 s on average per crystal. The end of data collection triggers an automatic data processing pipeline known as *AutoProcess* (provided by CLS) that uses the programs *XDS* (Kabsch, 2010) and *Pointless* (Evans, 2006). For ligand and drug screening experiments, the difference map can be automatically calculated by using *DIMPLE* (available through *CCP4*) just after the end of the *AutoProcess* analysis, when users provide a coordinate file of the search model through *MxLIVE* or under a reference folder in their home directory. The results of *DIMPLE* can be explored in *MxLIVE* through *UglyMol* (https://uglymol.github.io) [Fig. 4(*b*)]. The automatic data processing is performed by a high-performance computing cluster with 192-core processors. The data storage of the beamline is 140 TB over 10 GB s^{-1} connection with all the computers of the beamline. The user-account authorization is managed by Open LDAP in all computers. Remote access of the beamline has been allowed since the end of last year to increase the efficiency of MX experiments through the *NoMachine* NX software package (NoMachine, Luxembourg). Up to now, remote data collection is routinely performed by domestic or international users and accounts for approximately 60% of used beam time. In addition, users who are conducting on-site experiments can process and analyze their data by using commonly known software, including *HKL2000* (Otwinowski & Minor, 1997), *XDS* (Kabsch, 2010), *CCP4i* (Winn *et al.*, 2011), and *Phenix* (Adams *et al.*, 2010).

3. Facility access

The beamline facilities can be accessed by submitting a beam-time proposal three times a year via the website (http://pal.postech.ac.kr). The proposals are peer-reviewed and scored by an external panel based on their scientific significance and the technical feasibility of the research plan. Three types of proposals are available: (i) general proposals, which are only effective for one term and must be open to the public; (ii) long-term proposals, which last for two years and are also open to the public; and (iii) urgent request proposals, which can be submitted any time and are intended for important or urgent samples under the agreement of the beamline scientists. Industrial users can access the beamline through a fee-for-service program based on a mail-in service. In general, 70% of the total beam time is allocated for public users, whereas the remainder is used for beamline maintenance, upgrades, and industrial users who purchase beam time.

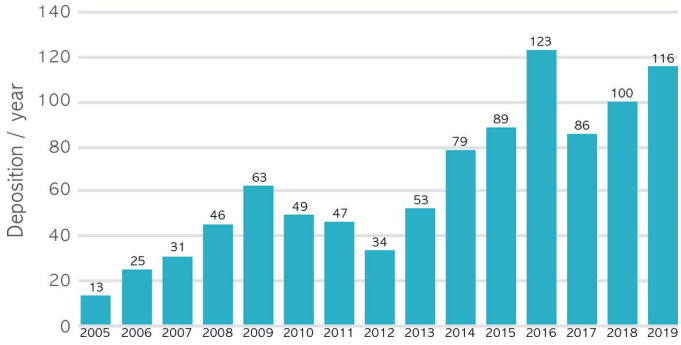

Figure 5
Histogram of the protein structure coordinates determined from BL-5C released per year from the PDB (the data were taken from the BioSync webpage, http://biosync.sbkb.org/).

4. Conclusion

BL-5C, one of the MX beamlines at Pohang Light Source-II, has been in full user operation since 2005 to meet the increasing beam time needs in the structural biology community in Korea. At the moment of writing this paper, 978 structures had been deposited in the Protein Data Bank (PDB) from BL-5C since its first user in 2005 (Fig. 5). To address industrial user's demand on high-throughput crystallography, the beamline has been intensively upgraded throughout the last two years to implement automated high-throughput data collection procedures. Most of the experimental setup and software of the beamline have been renewed to improve the throughput and reliability. Therefore, a throughput higher than 400 data sets collected under automated mode a day without interruption can be reached. The robot ISARA has been extensively commissioned to increase the robustness of the sample exchanging procedures. Now, the mounting/dismounting failure rate of the robot is below 0.1%. The high-capacity dewar accommodating up to 464 samples in the robot allows the beamline to run for 24 h without manual feeding of sample pucks during one day shift. The collected data sets are automatically analyzed by the *XDS*-based data processing pipeline *AutoProcess*. In addition, the difference map for ligand screening is calculated by using *DIMPLE*, and users can evaluate the results through a website. Our automatic data analysis pipeline combined with the difference map calculation minimizes the human input by eliminating the iterated data analysis process. This high-throughput capability and automatic data analysis of this beamline can contribute to facilitate the structure- or fragment-based drug design process of academic and industrial users.

Acknowledgements

The authors gratefully acknowledge those colleagues who formerly worked for the beamline from the beamline supporting group. In addition, special thanks to CMCF members who helped to implement the *MxDC*, *MxLIVE*, and *AutoProcess* beamline software.

Funding information

The following funding is acknowledged: This research was supported by the Bio & Medical Technology Development Program of the National Research Foundation (NRF) funded by the Korean government (MSIT) (No. NRF-2019M3E5D6063871).

References

Adams, P. D., Afonine, P. V., Bunkóczi, G., Chen, V. B., Davis, I. W., Echols, N., Headd, J. J., Hung, L.-W., Kapral, G. J., Grosse-Kunstleve, R. W., McCoy, A. J., Moriarty, N. W., Oeffner, R., Read, R. J., Richardson, D. C., Richardson, J. S., Terwilliger, T. C. & Zwart, P. H. (2010). *Acta Cryst.* D**66**, 213–221.
Bowler, M. W., Nurizzo, D., Barrett, R., Beteva, A., Bodin, M., Caserotto, H., Delagenière, S., Dobias, F., Flot, D., Giraud, T., Guichard, N., Guijarro, M., Lentini, M., Leonard, G. A., McSweeney, S., Oskarsson, M., Schmidt, W., Snigirev, A., von Stetten, D., Surr, J., Svensson, O., Theveneau, P. & Mueller-Dieckmann, C. (2015). *J. Synchrotron Rad.* **22**, 1540–1547.
Bowler, M. W., Svensson, O. & Nurizzo, D. (2016). *Crystallogr. Rev.* **22**, 233–249.
Bradley, A., Skyner, R. & von Delft, F. (2018). *Abstracts Papers Am. Chem. Soc.* Vol. 255.
Brockhauser, S., Ravelli, R. B. G. & McCarthy, A. A. (2013). *Acta Cryst.* D**69**, 1241–1251.
Casanas, A., Warshamanage, R., Finke, A. D., Panepucci, E., Olieric, V., Nöll, A., Tampé, R., Brandstetter, S., Förster, A., Mueller, M., Schulze-Briese, C., Bunk, O. & Wang, M. (2016). *Acta Cryst.* D**72**, 1036–1048.
Cianci, M., Bourenkov, G., Pompidor, G., Karpics, I., Kallio, J., Bento, I., Roessle, M., Cipriani, F., Fiedler, S. & Schneider, T. R. (2017). *J. Synchrotron Rad.* **24**, 323–332.
Dalesio, L. R., Hill, J. O., Kraimer, M., Lewis, S., Murray, D., Hunt, S., Watson, W., Clausen, M. & Dalesio, J. (1994). *Nucl. Instrum. Methods Phys. Res. A*, **352**, 179–184.
Evans, G. & Pettifer, R. F. (2001). *J. Appl. Cryst.* **34**, 82–86.
Evans, P. (2006). *Acta Cryst.* D**62**, 72–82.
Fodje, M., Janzen, K., Berg, R., Black, G., Labiuk, S., Gorin, J. & Grochulski, P. (2012). *J. Synchrotron Rad.* **19**, 274–280.
Giraud, T., Dobias, F., Gabadinho, J., Rey-Bakaikoa, V., Nurizzo, D., Leonard, G. A. & Mueller-Dieckmann, C. (2009). *J. Appl. Cryst.* **42**, 125–128.
Hirata, K., Yamashita, K., Ueno, G., Kawano, Y., Hasegawa, K., Kumasaka, T. & Yamamoto, M. (2019). *Acta Cryst.* D**75**, 138–150.
Hwang, I., Huang, J. Y., Kim, M., Lee, B., Kim, C., Choi, J., Kim, M., Lee, H. S., Moon, D., Lee, E. H., Kim, D., Nam, S. H., Shin, S. & Cho, M. (2014). *Rev. Sci. Instrum.* **85**, 055113.
Kabsch, W. (2010). *Acta Cryst.* D**66**, 125–132.
Ko, J., Kim, I.-Y., Kim, C., Kim, D.-T., Huang, J.-Y. & Shin, S. (2016). *J. Synchrotron Rad.* **23**, 448–454.
Lima, G. M. A., Talibov, V. O., Jagudin, E., Sele, C., Nyblom, M., Knecht, W., Logan, D. T., Sjögren, T. & Mueller, U. (2020). *Acta Cryst.* D**76**, 771–777.
Otwinowski, Z. & Minor, W. (1997). *Method Enzymol.* **276**, 307–326.
Owen, R. L., Holton, J. M., Schulze-Briese, C. & Garman, E. F. (2009). *J. Synchrotron Rad.* **16**, 143–151.
Park, J. Y., Kim, Y., Lee, S. & Lim, J. (2018). *J. Synchrotron Rad.* **25**, 869–873.
Sanchez-Weatherby, J., Sandy, J., Mikolajek, H., Lobley, C. M. C., Mazzorana, M., Kelly, J., Preece, G., Littlewood, R. & Sørensen, T. L.-M. (2019). *J. Synchrotron Rad.* **26**, 291–301.
Sato, K. (2001). *J. Synchrotron Rad.* **8**, 378–380.
Wasserman, S. R., Koss, J. W., Sojitra, S. T., Morisco, L. L. & Burley, S. K. (2012). *Trends Pharmacol. Sci.* **33**, 261–267.

Winn, M. D., Ballard, C. C., Cowtan, K. D., Dodson, E. J., Emsley, P., Evans, P. R., Keegan, R. M., Krissinel, E. B., Leslie, A. G. W., McCoy, A., McNicholas, S. J., Murshudov, G. N., Pannu, N. S., Potterton, E. A., Powell, H. R., Read, R. J., Vagin, A. & Wilson, K. S. (2011). *Acta Cryst.* D**67**, 235–242.
Winter, G., Waterman, D. G., Parkhurst, J. M., Brewster, A. S., Gildea, R. J., Gerstel, M., Fuentes-Montero, L., Vollmar, M., Michels-Clark, T., Young, I. D., Sauter, N. K. & Evans, G. (2018). *Acta Cryst.* D**74**, 85–97.
Wojdyla, J. A., Panepucci, E., Martiel, I., Ebner, S., Huang, C.-Y., Caffrey, M., Bunk, O. & Wang, M. (2016). *J. Appl. Cryst.* **49**, 944–952.
Yu, C.-J., Lee, H. C., Kim, C., Cha, W., Carnis, J., Kim, Y., Noh, D. Y. & Kim, H. (2014). *J. Synchrotron Rad.* **21**, 264–267.